

Article

# Estimation of 10-Hour Fuel Moisture Content Using Meteorological Data: A Model Inter-Comparison Study

HoonTaek Lee <sup>1</sup> , Myoungsoo Won <sup>2,\*</sup>, Sukhee Yoon <sup>1</sup> and Keunchang Jang <sup>1</sup>

<sup>1</sup> Division of Forest Ecology and Climate Change, National Institute of Forest Science, Seoul 02455, Korea; lht3718@gmail.com (H.L.); skyoon337@korea.kr (S.Y.); kcjang@korea.kr (K.J.)

<sup>2</sup> Division of Forest Restoration and Resource Management, National Institute of Forest Science, Seoul 02455, Korea

\* Correspondence: forestfire@korea.kr

Received: 28 July 2020; Accepted: 8 September 2020; Published: 11 September 2020



**Abstract:** Forest fire modeling often requires estimates of fuel moisture status. Among the various fuel variables used for fire modeling studies, the 10-h fuel moisture content (10-h FMC) is a promising predictor since it can be automatically measured in real time at study sites, yielding more information for fire models. Here, the performance of 10-h FMC models based on three different approaches, including regression ( $M_{REG}$ ), machine learning algorithms ( $M_{ML}$ ) with random forest and support vector machine, and a process-based model ( $M_{FSMM}$ ), were compared. In addition, whole-year models of each type were compared with their respective seasonal models to explore whether the development of separate seasonal models yielded better estimates. Meteorological conditions and 10-h FMC were measured each minute for 18 months in and near a forest site and used for constructing and examining the 10-h FMC models. In the assessments,  $M_{ML}$  showed the best performance ( $R^2 = 0.77$ – $0.82$  and root mean squared error [RMSE] =  $2.05$ – $2.84\%$ ). The introduction of the correction coefficient into  $M_{REG}$  improved its estimates ( $R^2$  improved from  $0.56$ – $0.58$  to  $0.68$ – $0.70$  and RMSE improved from  $3.13$ – $3.85\%$  to  $2.64$ – $3.27\%$ ) by reducing the errors associated with high 10-h FMC values.  $M_{FSMM}$  showed the worst performance ( $R^2 = 0.41$ – $0.43$  and RMSE =  $3.70$ – $4.39\%$ ), which could possibly be attributed to the lack of radiation input from the study sites as well as the particular fuel moisture stick sensor that was used. Whole-year models and seasonal models showed almost equal performance because 10-h FMC varied in response to atmospheric moisture conditions rather than specific seasonal patterns. The adoption of a hybrid modeling approach that blends machine-learning and process-based approaches may yield better predictability and interpretability. This study provides additional evidence of the lagged response of 10-h FMC after rainfall, and suggests a new way of accounting for this response in a regression model. Our approach using comparisons among models can be utilized for other fire modeling studies, including those involving fire danger ratings.

**Keywords:** fuel moisture content; meteorological data; regression; machine learning; process-based model; forest fire

## 1. Introduction

Dead fuel moisture content (FMC) is an important factor in forest fire research and in operational systems for fire danger rating or fire behavior because it affects not only the occurrence, spread, and intensity of the forest fire, but also the survival of vegetation near the fire [1]. Dead fuel can be divided into four categories (1-, 10-, 100-, and 1000-h fuels) based on the response time (or time lag) concept [2]. The numbers indicate the approximate time in hours necessary for a given size fuel to lose 63% ( $1 - e^{-1}$ ) of the difference between its initial moisture content and its equilibrium moisture content

(EMC), and are related to fuel size [3]. For example, 10-h fuel usually refers to fuel with diameter ranging from 0.64 to 2.54 cm [4]. Fuel moisture content is usually measured by a manual oven-drying process e.g., [5–7]. However, 10-h FMC can be measured automatically under near-real-time conditions by using a commercial standardized fuel stick sensor, e.g., [8–10].

Many studies have estimated FMC by using empirical and process-based models [11]. Empirical models are constructed using statistical methods such as linear regression, in which a variety of input variables such as weather, fuel, and stand characteristics are related to the FMC [6]. In particular, the EMC has been traditionally used as a predictor for vapor exchange processes by fuel [12], and is thus used within fuel moisture models e.g., [13–15]. In contrast, process-based models depict physical processes that occur within and around the fuel, such as heat and mass fluxes, to estimate FMC, e.g., [4,9,13,16–20]. Among process-based models, those proposed by Nelson [16] and van der Kamp et al. [9] were aimed at estimating FMCs of various sizes including 10-h fuel, while others attempted to estimate litter moisture content. Nelson’s model was adopted by the National Fire Danger Rating System (USA), and van der Kamp et al. [9] partly modified Nelson’s model.

The use of supervised machine-learning algorithms represents another potential approach for estimating FMC. This approach has widely been used in forest fire research, including studies pertaining to fire danger ratings [21–23], fire detection [24], fire ignition distribution [25], and analysis of the burned area and severity [26–30]. However, to the best of our knowledge, no previous study has applied machine learning methods to estimate the moisture content of any size dead fuel, including 10-h FMC. Since approaches based on supervised machine-learning algorithms have shown competitive performance in other areas of forest fire research, their applicability to 10-h FMC estimation deserves to be tested.

The three methods mentioned above can be used to estimate FMC and improve existing fire danger rating or fire behavior systems. For example, they can be used to improve the Korea Forest Fire Danger Rating [31], a fire danger rating system operated by the National Institute of Forest Science (NIFoS) of Republic of Korea. This system assesses current fire danger by using an index in which relative humidity and effective humidity (Section 2.2) are used as proxies for moisture status relative to forest fire occurrence [31]. However, instead of proxies that are based on atmospheric conditions, FMC can more directly and realistically represent the fuel moisture status. Soil moisture deficit (SMD) has also been utilized as an indicator of FMC [32], but SMD is reported to be incapable of representing FMC [33]. Thus, FMC estimates, and thereby fire models, may be improved by replacing these proxies with FMC itself. However, optimal measurements and estimates of FMC are essential to attempt these improvements.

The purpose of this study is to compare the performance of several 10-h FMC models that use meteorological variables as the input. To this end, 10-h FMC was measured using the fuel stick sensors at two sites; the 10-h FMC and weather datasets were used to build a novel regression model that considers the lagged drying response of 10-h FMC after rainfall; and the performance of this model was compared to those of a process-based model and machine-learning models.

## 2. Materials and Methods

### 2.1. Study Sites

Datasets from two automatic weather station (AWS) sites were used (Figure 1). One of the two sites was installed in Hongneung Forest (HFI, 37°35′44.16″ N, 127°2′42.71″ E, 60 m a.s.l.), a temperate forest dominated by Korean red pine (*Pinus densiflora* Siebold et Zucc), while the other was located outside Hongneung Forest (HFO, 37°35′37.7″ N, 127°2′34.1″ E, 35 m a.s.l.). In 2019, the annual rainfall in HFI was 756.0 mm and air temperature was 13.1 °C ± 10.4 °C (mean ± standard deviation [SD]; range, −10.2 °C to 35.4 °C). In HFO, annual rainfall was 870.3 mm, and mean ± SD air temperature was 13.0 °C ± 10.7 °C (range, −10.2 °C to 36.0 °C). Meteorological variables, including air temperature, relative humidity, wind speed, wind direction, air pressure, land surface temperature, and rainfall

intensity, were observed at both sites. In addition, 10-h FMC was observed using an FS-3 fuel stick (FST, Victoria, British Columbia, Canada). The FS-3 fuel stick was installed 30 cm above the ground heading to the north [10]. The fuel stick was made of ponderosa pine (*Pinus ponderosa*) and has been widely used to measure 10-h FMC [9,33,34]. It can range up to 28% while actual 10-h FMC can range up to about 60%. In spite of this mismatch in the ranges, the FS-3 fuel stick was used here because this study aims at research topics about forest fires, for which the lower range of 10-h FMC is most important.

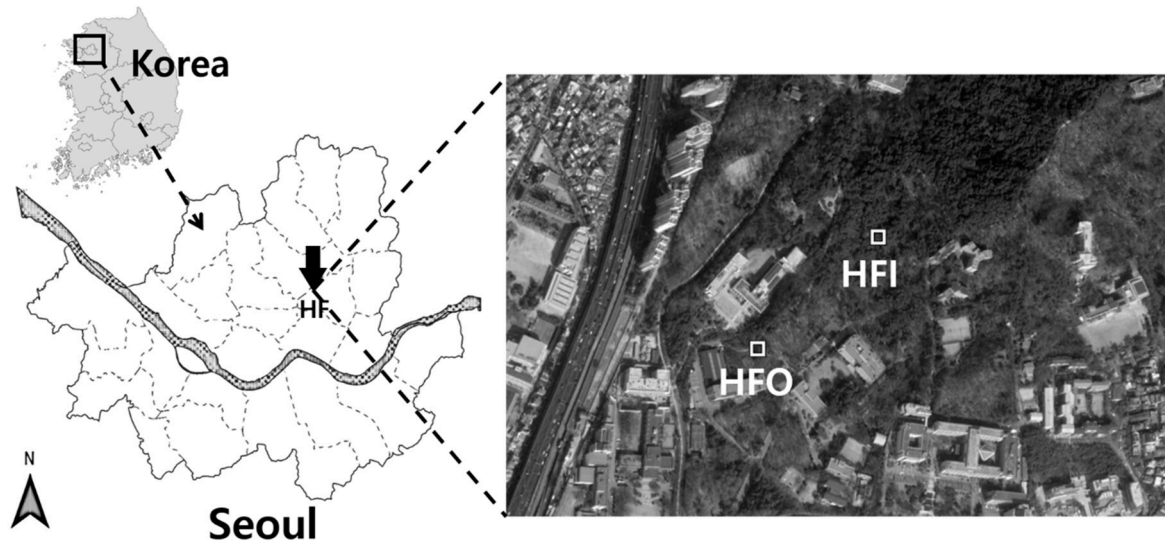


**Figure 1.** Location of the two study sites (HFI and HFO) in Hongneung Forest.

## 2.2. Data

The study period was from September 2018 to February 2020. Meteorological variables were measured and used as predictors or forcing variables in the 10-h FMC models. Air temperature, relative humidity, and wind speed and direction were measured at 2 and 10 m above the ground; the measurements obtained at 2 m were used for the model input on the basis of the assumption that they represent the surface weather conditions better. Secondary variables such as EMC (Appendix A: Equation (A1)–(A5)), effective humidity (EH, Equation (A6)), and vapor pressure deficit (VPD, Equation (A7)–(A8)) were computed from the directly observed variables. EMC and VPD were derived from air temperature ( $T_a$ , °C) and relative humidity ( $RH_a$ , %). EH represents the dryness of wood and it is computed from the  $RH_a$  of the last 5 days [35]. In addition to the meteorological variables, the FS-3 fuel stick measured the relative humidity and temperature inside the stick, and the 10-h FMC was calculated from these two variables by using an equation provided by the manufacturer (Equation (A9)). All measurements were recorded each minute, and then aggregated to obtain hourly measurements for model construction and further analysis.

## 2.3. Models Considered

Three types of 10-h FMC models were taken into consideration. The first type was a simple regression model based on EMC that was proposed by Lee et al. [10]. This regression model was modified to attenuate the effect of an error source: delayed drying of 10-h FMC as compared to EMC after rainfall. In the second approach, random forest (RF) and support vector machine (SVM) techniques were deployed to construct a 10-h FMC model. For each technique, meteorological variables selected by a feature selection method were used as independent variables. For the third approach, the fuel stick moisture model (FSMM) by van der Kamp et al. [9] was considered. This process-based model is a modified version of the original model proposed by Nelson [16], with the modifications including a more sophisticated radiation transfer scheme and simplified evaporation process. The authors verified

that their modified model showed better performance than the original model and could consider canopy coverage and sky conditions more realistically [9].

### 2.3.1. Model 1—Regression Models Using Equilibrium Moisture Content (EMC) and a Correction Coefficient ( $M_{REG}$ : REG and $REG_{COR}$ )

The first model used a simple linear regression method with EMC as the predictor of 10-h FMC (hereafter, REG):

$$10\text{-h FMC} = a + b \times EMC \quad (1)$$

where  $a$  and  $b$  are regression coefficients.

Although the 10-h FMC can be adequately estimated by using EMC alone, the model based on EMC alone showed a significant error, which appeared for a few days after the end of each rainfall and faded with time [9]. On the basis of this observation, a correction coefficient (CC) was added to the predictor space to alleviate the uncertainty, creating a new regression formula (hereafter,  $REG_{COR}$ ).

The CC of  $REG_{COR}$  was derived from a curve (hereafter, CC curve) relating the difference between 10-h FMC and EMC ( $diff_{EMC,FMC}$ ) and the number of hours after the end of rainfall ( $hrs_{norain}$ ). The  $diff_{EMC,FMC}$  was calculated by subtracting 10-h FMC from EMC for each hour. The  $hrs_{norain}$  was calculated by accumulating the number of hours from the time since the last rainfall, and was set back to zero when the hourly rainfall amount was more than zero. For each site, the CC curve was fitted as follows:

$$diff_{EMC,FMC} = a + b \times \log h_{norain} \quad (2)$$

where  $a$  and  $b$  are regression coefficients. The resultant CC curves of the two sites were compared using Chow's test to determine if they were different [36]. The test was conducted in R [37] using the "gap" package [38].

Notably, the range of  $h_{norain}$  values used for fitting can affect the curve shape; if a large upper limit is allowed for  $h_{norain}$ , the resultant prolonged no-rainfall period will form a tail (Figure 2). However, in a preliminary analysis, this effect was verified to be trivial at an  $R^2$  difference of 0.03. Moreover, the range of  $h_{norain}$  values used in the fitting needed to be sufficiently wide to allow extrapolation to other sites. Therefore, the maximum  $h_{norain}$  value for each site (731 for HFI and 847 for HFO) was used for fitting the CC curve. In addition, hourly measurement records with an  $h_{norain}$  value of zero were excluded from the fitting to avoid negative infinite  $diff_{EMC,FMC}$ . The estimated  $diff_{EMC,FMC}$  was determined as the CC for each timestep and used as an additional independent variable for REG:

$$10\text{-h FMC} = a + b \times EMC + c \times diff_{EMC,FMC} \quad (3)$$

where  $a$ ,  $b$ , and  $c$  are regression coefficients.

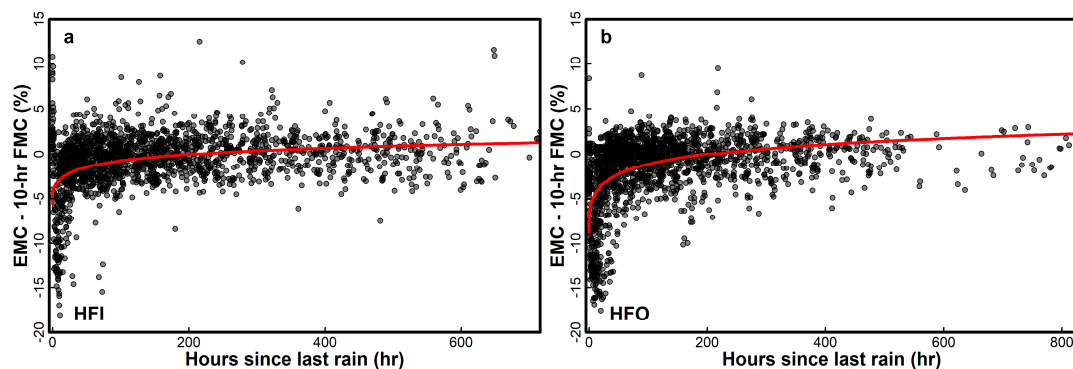


**Figure 2.** Fitted relationships (red curves) between the number of hours since the last rain and the difference between equilibrium moisture content (EMC) and 10-h fuel moisture content (10-h FMC) for two sites (a for HFI and b for HFO). A test dataset was used for plotting (see Section 2.4).

### 2.3.2. Model 2—Supervised Machine-Learning Methods ( $M_{ML}$ )

#### Random Forest

Random forest is a popular machine-learning technique based on the classification and regression tree (CART) methodology [39]. RF is an ensemble of many regression trees built using bootstrapped training data whose size is usually two-thirds of the entire data. For each tree, RF uses a subset of all available predictors with a predefined size (*mtry*) [40]. The use of a subset of predictors decreases the correlation among decision trees in RF, making the ensemble of the trees more reliable [40]. The number of parameters that require tuning in RF is relatively small. The default value 5 was used as the minimum node size for each tree. The number of trees to grow (*ntree*) was set to 1000, as recommended by Kuhn and Johnson [41]. This value is a practical starting point that offers a balance between computational cost and stable performance. The *mtry* value was tuned using the “caret” package in R [42]. RF was implemented using the “randomForest” package in R [43].

#### Support Vector Machine

Support vector machine is a machine-learning technique that is used for both classification and regression problems [44]. SVM is basically an algorithm to find separating hyperplanes in a feature space. SVM uses a kernel function by which the existing feature space is mapped into a higher-dimensional space, which makes it easier for SVM to find the best hyperplane and resolve even non-linear problems [45]. A radial basis function was used in this study because it has been shown to outperform other kernels in various prediction studies [22,46,47]. Identification of the separating hyperplane involves a loss function and penalty. In this study, SVM regression with the  $\epsilon$ -insensitive loss function ( $\epsilon$ -SVR) was used [48]. The  $\epsilon$ -SVR constructs the best hyperplane in the feature space while ignoring points within  $\pm\epsilon$ . A penalty parameter (*cost*) was used as a budget for the ignorance, that is, larger residuals are penalized by consuming a larger part of this budget [41]. The two parameters  $\epsilon$  and *cost* were tuned by the “caret” package in R [42]. The  $\epsilon$ -SVR was performed within the “kernlab” package in R [49].

#### Feature Selection

Feature selection can improve model performance by alleviating the problems imposed by dimensionality and saving computational cost [46,50]. In this study, recursive feature elimination (RFE), a backward feature selection algorithm [51], was used for feature selection. RFE is a feature selection algorithm that not only effectively reduces the dimensionality of a model, but it is also robust to the overfitting problem [51]. RFE constructs a full model using all predictors and evaluates its performance. Then, it removes the least important predictor from the full model, and then trains and evaluates a new model using the remaining predictors. This process is performed iteratively until only one predictor remains in the model. Finally, the best model with a specific subset of predictors is determined on the basis of an evaluation metric. All available variables from our measurements were considered for the full model in RFE to fully exploit our information. The importance of each predictor was measured by a built-in measure of predictor importance (RF variable importance) for RF and a filter approach using the locally weighted regression model for SVM [42]. Development and evaluation of the model were performed by applying five repeats of 10-fold cross validation as a resampling method. The root mean squared error (RMSE) was used as a metric for the predictor importance. RFE was conducted using the *rfe()* function of the “caret” package in R [42]. RF and SVM were also implemented by the *rfe()* function while specifying each learning algorithm to use. Model tuning and evaluation were concurrently performed in RFE, and the resultant model and performance scores ( $R^2$  and RMSE) were used for further analysis.

### 2.3.3. Model 3—Fuel Stick Moisture Model (FSMM) ( $M_{FSMM}$ )

The FSMM is a process-based model used for estimating FMC in fuels of various sizes, including 10-h fuel [9]. The source code of the model is freely accessible at a Github repository [52]. It currently lacks modules for several functions, including shortwave partitioning, obtaining the sun position, and computing the downward longwave radiation, all of which were implemented in R by referring to the equations in the descriptive paper [9]. Several parameter values were modified, since the fuel stick sensors used by van der Kamp et al. [9] differed from those used in the current study. The maximum value that the FSMM can produce was decreased to 30%; the radius ( $r$ ) and length ( $L$ ) of the fuel stick were changed from 0.0065 to 0.0125 m and from 0.41 to 0.13 m, respectively. However, fuel stick density ( $RHO\_S$ ) was not modified from the original value ( $400 \text{ kg m}^{-3}$ ) because the two types of sensors were made of the same tree species (*Pinus ponderosa*).

The particle swarm optimization method was implemented using the *psoptim()* function of the “pso” package in R [53] to optimize five parameters of the FSMM (Table 1). For the parameter  $f$ , which represents the stick volume fraction taken up by an outer layer of fuel in FSMM, a constant value (0.28) was predefined during the optimization, in accordance with the approach proposed by van der Kamp et al. [9]. The number was derived from averaging optimized  $f$  of both sites and seasons (whole year and each season). The diffusivity coefficient,  $d_s$ , was freely adjusted regardless of its reported range from previous studies since it does not need to be constrained within a range in FSMM [9]. The other three parameters ( $A$ ,  $B$ ,  $m_{max}$ ) were adjusted within the range used by van der Kamp et al. [9]. RMSE was used as an objective metric of optimization. Optimization was assumed to be complete when there was no improvement for over 20 consecutive iterations; default values were used for other options. All meteorological and 10-h FMC datasets needed for the FMC models were retrieved from the two sites, HFO and HFI. Notably, the total downward shortwave radiation was retrieved from the nearest weather observatory (the Seoul Meteorological Observatory; c. 8 km southwest of HFI and HFO) and applied to both sites. This could be problematic because HFI is shaded by the Pine canopy. However, we used the radiation data set because (1) it was our best available one and (2) it would be sufficient for explore the feasibility of the FSMM to estimate 10-h FMC over the two sites and for comparing its performance with those of other models.

**Table 1.** Optimal parameter values of the 10-h fuel moisture models (REG: regression model, CC curve: correction coefficient curve, REG<sub>COR</sub>: regression model with a correction coefficient, and FSMM: fuel stick moisture model).  $a$ ,  $b$ , and  $c$  are regression coefficients;  $A$  and  $B$  are empirical constants related to the equilibrium moisture content;  $d_s$  ( $\text{m}^{-2} \text{s}^{-1}$ ) is a coefficient indicating bulk moisture diffusion for the entire stick;  $m_{max}$  (fraction) is the maximum allowable moisture content (fraction);  $f$  is the stick volume taken up by the outer layer (fraction). Whole year refers to the entire data period; FS1, to February through May; WS, to June through October; and FS2, to November through January.

		REG		CC Curve		REG <sub>COR</sub>			FSMM				
		$a$	$b$	$a$	$b$	$a$	$b$	$c$	$A$	$B$	$d_s$	$m_{max}$	$f$
HFI	Whole year	2.89	0.82	−5.61	1.04	2.98	0.72	−1.29	4.59	−10.00	$3.23 \times 10^{-9}$	0.38	0.28
	FS1	3.53	0.69	−5.20	0.97	3.67	0.63	−1.30	4.84	−12.56	$2.39 \times 10^{-9}$	0.38	0.28
	WS	3.20	0.84	−5.89	1.12	2.70	0.78	−1.16	5.15	−13.62	$3.21 \times 10^{-9}$	0.38	0.28
	FS2	2.93	0.79	−5.67	1.03	3.18	0.68	−1.34	4.62	−10.70	$3.83 \times 10^{-9}$	0.41	0.28
HFO	Whole year	0.91	1.07	−8.79	1.64	0.61	0.95	−1.00	4.59	−10.00	$3.22 \times 10^{-9}$	0.38	0.28
	FS1	1.35	0.99	−8.78	1.72	1.12	0.89	−1.02	4.56	−10.15	$2.20 \times 10^{-9}$	0.38	0.28
	WS	0.52	1.14	−8.65	1.64	−0.45	1.06	−0.92	4.69	−10.00	$4.15 \times 10^{-9}$	0.36	0.28
	FS2	1.55	0.99	−9.84	1.75	1.54	0.84	−1.09	4.54	−10.00	$7.87 \times 10^{-9}$	0.40	0.28

### 2.4. Model Evaluation

To evaluate and compare the three methods, the whole dataset (meteorological and 10-h FMC measurements) for each site was divided into two parts, training (80%) and test (20%). The whole data were classified into three groups based on a plot relating rainfall duration and rainfall intensity to

the 10-h FMC (Figure 3). Rainfall duration was used as the grouping criteria because over 80% of the data points occurred within the first three hours (vertical dotted lines in Figure 2a,b) from the start of rainfall events. Although Vinney [12] reported that 2 mm of hourly rainfall is sufficient to saturate fuel, many of our observations remained unsaturated at intensity values over 2 mm/hour (vertical dotted lines in Figure 3c,d). This may have occurred because an intense rain is typically of short duration and does not result in water remaining on the fuel as long as with a slower rain, which implies that it is the rainfall duration, rather than intensity, which is more critical. Times with no rainfall constituted group (a), data with rainfall duration of less than 3 h constituted the second group (b), while the rest of the data were categorized in the third group (c). Stratified random sampling was used to split the entire data into training and test datasets, and the size of each group was used as a weight factor for sampling. The training set was used to build the 10-h FMC models, which were applied to the test set to evaluate and compare their performance. This method ensured that all models were impartially compared by using the same input data.  $R^2$  and RMSE were used as measures for model performance.

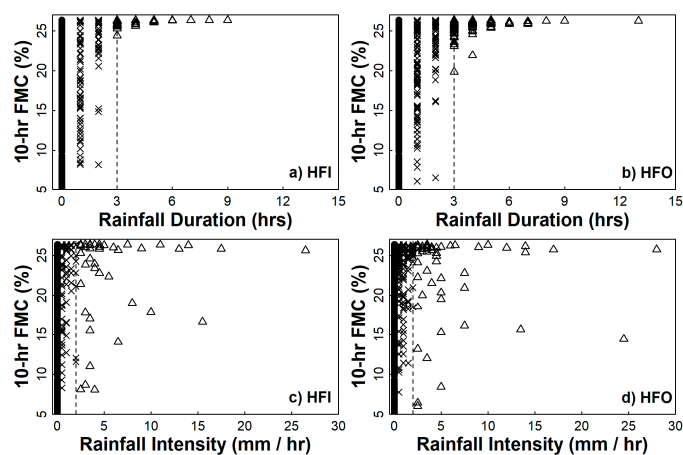


**Figure 3.** Relationships between 10-h fuel moisture content (10-h FMC) and rainfall duration (a,b) and rainfall intensity (c,d). Using each variable, the entire data was split into three groups: (1) rainfall duration = 0 (circles), 0 < rainfall duration < 3 (crosses), and rainfall duration > 3 (triangles), and (2) rainfall intensity = 0 (circles), 0 < rainfall intensity < 2 (crosses), and rainfall intensity > 2 (triangles).

Model estimates for 10-h FMC observations below 10% were also evaluated because approximately 70% of recent forest fires occurred with 10-h FMC below 10% [10]. We named models using the entire data period (i.e., from September 2018 to February 2020) as “whole year” models. In addition, seasonal models were constructed, run, and examined using the same approach to explore whether the development of seasonal models improved predictability. The Korean government specifies two fire seasons and the Korea Forest Fire Danger Rating uses different submodels for the two seasons. Because a possible opportunity resulted from this study is to incorporate the resulted model into the fire danger rating system, we divided the year into three seasons: two fire seasons (FS1: February–May and FS2: November–January) and a wet season (WS: June–October). More than two-thirds of annual rainfall in 2019 fell during the wet season (68.0% and 66.9% for HFI and HFO, respectively). For the last 20 years, there has been an average of 448 fire occurrences per year in Korea, of which over 90% occurred during the two fire seasons [54].

### 3. Results

#### 3.1. 10-h Fuel Moisture Content (FMC) Measurements

The 10-h FMC measurements in HFI generally showed higher median values with lower variability in comparison with the measurements in HFO (Table 2), which can be attributed to radiation interception by the canopy [10,11,19]. The minimum 10-h FMC value was 4.97% in HFI and 3.50% in HFO;

the maximum value was 26.36% for both sites. Generally, the lower range of 10-h FMC was from 5% to 10% during the fire seasons, while the WS, which received more than half of the annual rainfall amount (68.0% for HFI and 66.9% for HFO), showed higher 10-h FMC (10% to 15%) in its lower range of values. The moisture content rapidly increased to more than 25% and decreased to the normal range in response to the start and end of rainfall events.

**Table 2.** Summary of the 10-h fuel moisture content measurements (%) during each period. Whole year refers to the entire data period; FS1, to February through May; WS, to June through October; and FS2, to November through January.

	HFI					HFO				
	Min	Median	Max	Mean	SD	Min	Median	Max	Mean	SD
Whole year	4.97	10.89	26.36	12.32	4.85	3.50	10.66	26.36	12.53	5.83
FS1	4.97	9.81	26.36	10.66	4.51	3.50	9.15	26.34	10.87	5.57
WS	6.63	12.81	26.36	14.29	4.79	3.92	12.94	26.36	14.47	5.84
FS2	5.82	10.36	26.36	11.52	4.44	4.24	10.14	26.36	11.77	5.40

### 3.2. Model Fitting

For  $M_{REG}$  with the test dataset, the  $diff_{EMC,FMC}$  showed strong negative values up to  $-18.9\%$  some hours from the end of rainfall, after which it increased to around zero and fluctuated with time (Figure 2). HFO contained many more points with negative  $diff_{EMC,FMC}$  values than HFI. As a result, the CC curve of HFO contained more negatively fitted values at around  $hrs_{norain}$  of zero and a more negative minimum value of CC. The CC ranged from  $-8.79\%$  to  $2.21\%$  in HFO and from  $-5.60\%$  to  $1.23\%$  in HFI. The majority ( $>69\%$ ) of the resultant CC values were strongly negative around  $hrs_{norain}$  of zero, and in Table 1, all  $c$  values were negative. Thus, the CC in  $REG_{COR}$  primarily functioned to increase 10-h FMC estimates after the end of rainfall, consistent with the purpose of the CC (i.e., reducing the estimation error after the end of rainfall). According to Chow's test, the CC curves of HFI and HFO differed from each other ( $p < 0.001$ ).

After training the model, the RFE algorithm reduced the dimensionality of the predictor space for each site and learning method except for SVM in HFI (Table 3). There were nine common predictors, namely, mean air temperature, land surface temperature, average and maximum wind direction and speed, air pressure, average relative humidity, and effective humidity (filled circles in Table 3) for all four cases (two learning methods  $\times$  two sites). EMC was selected only by SVM, although it showed the strongest correlation with 10-h FMC at both sites [10].

**Table 3.** Selected meteorological variables by the recursive feature elimination algorithm. Filled circles are common variables selected for both sites (HFI and HFO) and machine-learning algorithms (random forest (RF) and support vector machine (SVM)).

Variable	Description	HFI		HFO	
		RF (9)	SVM (13)	RF (10)	SVM (12)
TA_2_AVG	Average air temperature at 2 m height	•	•	•	•
LST	Land surface temperature	•	•	•	•
WS_2_AVG	Average wind speed at 2 m height	•	•	•	•
WS_2_MAX	Maximum wind speed at 2 m height	•	•	•	•
WD_2_AVG	Average wind direction at 2 m height	•	•	•	•
WD_2_MAX	Maximum wind direction at 2 m height (the maximum value for each hour)	•	•	•	•
PRESS	Air pressure	•	•	•	•
RH_2_AVG	Average relative humidity at 2 m height	•	•	•	•
EH	Effective humidity	•	•	•	•
VPD	Vapor pressure deficit		○	○	○
EMC	Equilibrium moisture content		○		○
RAIN	Hourly rainfall		○		
RAIN_DUR	Consecutive rainy hours		○		○

The trained optimal parameter values of FSMM by the particle swarm optimization method are presented in Table 1. The coefficient  $A$  was larger in HFI than in HFO and largest for the WS at both sites. These tendencies also appeared for the absolute values of coefficient  $B$  in HFI, but the  $B$  values in HFO were saturated or almost saturated to the upper limit of the available range. The  $m_{max}$  values were optimized to around 0.3, which is the upper bound of the fuel stick sensor, although the parameter was allowed to vary up to 1.5 during the optimization.

### 3.3. Model Performance

Incorporation of the CC into REG improved the fitness of the model for both sites (Figure 4a–d). The degree of improvement was comparable between both sites, although the model performance was better in HFI than in HFO. In HFI, the  $R^2$  of REG<sub>COR</sub> increased from 0.58 to 0.70 and RMSE decreased from 3.13% to 2.64% for the whole year, in comparison with REG. In HFO,  $R^2$  increased from 0.56 to 0.68 and RMSE decreased from 3.85% to 3.27% for the whole year. The time series pattern of the 10-h FMC estimates corresponded well with that of observations for HFI and HFO (Figure 5). REG notably underestimated 10-h FMC when it was more than  $c.$  20%. The underestimation occurred more frequently for HFO, making the fitness worse than that for HFI. These errors for high 10-h FMC in REG were attenuated in REG<sub>COR</sub> (Figure 5). REG and REG<sub>COR</sub> performed better than  $M_{FSMM}$  and performed worse than  $M_{ML}$ .

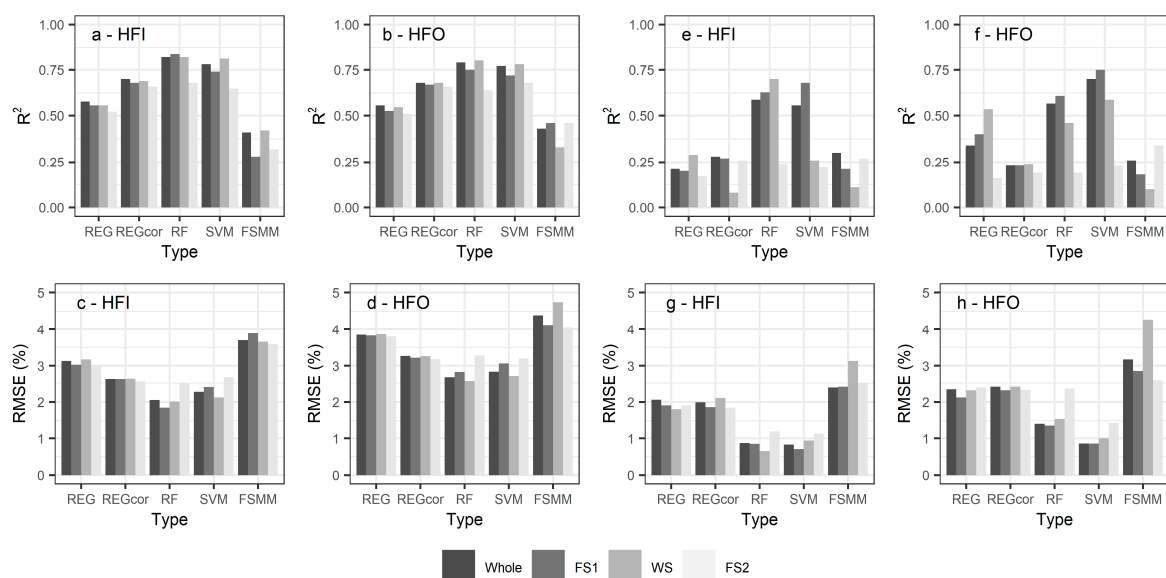


**Figure 4.** Model performances for each site/period combination of the whole range of 10-h fuel moisture contents (a–d) and observations less than 10% (e–h). Evaluation statistics are as follows: the coefficient of determination ( $R^2$ ) and the root mean squared error (RMSE). Whole refers to the entire data period; FS1, to February through May; WS, to June through October; and FS2, to November through January.

$M_{ML}$  showed the best fitness among the three model types for both sites, and RF showed slightly better performance than SVM for most cases (Figure 4a–d). In HFI, the whole-year model's  $R^2$  was 0.82 for RF and 0.78 for SVM. RMSE was 2.05% for RF and 2.27% for SVM. Like  $M_{REG}$ , there was a small decrease in the fitness in HFO.  $R^2$  was 0.79 for RF and 0.77 for SVM. RMSE was 2.69% for RF and 2.84% for SVM. The model's estimates of the 10-h FMC and observations showed a strongly bound time series pattern (Figure 6). The estimates were generally akin to observations, while there were underestimations for the high 10-h FMC.

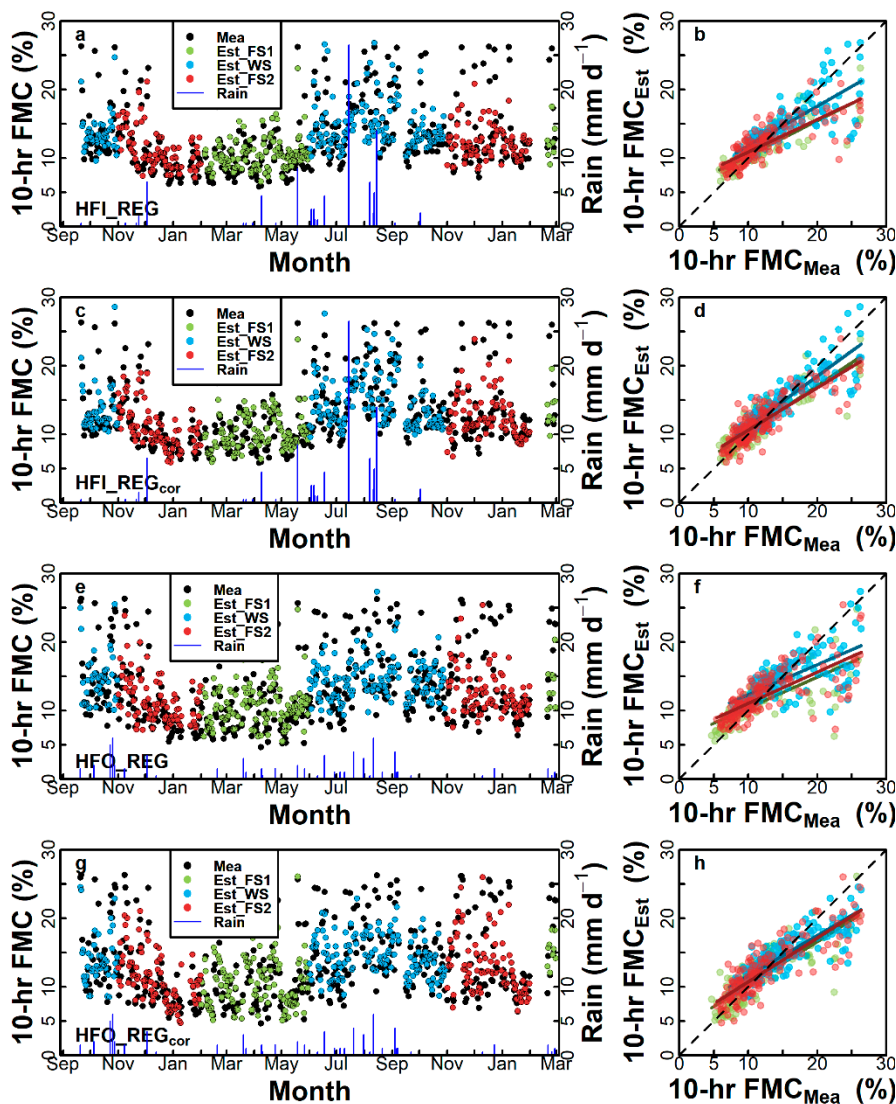


**Figure 5.** Time series and scatter plots comparing measurements (Mea) and estimates (Est) of 10-h fuel moisture content (10-h FMC) at HFI (a–d) and HFO (e–h) for each season: regression models ( $M_{REG}$ ). FS1 refers to February through May; WS, to June through October; and FS2, to November through January. To greatly reduce the number of data points appearing on the graph, daily mean 10-h FMC values of the test dataset were used.

$M_{FSMM}$  showed the worst performance among the three types of models (Figure 4a–d). In HFI, the whole-year model’s  $R^2$  was 0.41 and RMSE was 3.70%; in HFO,  $R^2$  was 0.43 and RMSE was 4.39%. Unlike  $M_{REG}$  and  $M_{ML}$ , both  $R^2$  and RMSE generally increased in HFO. For both HFI and HFO, the model overestimated low 10-h FMC, *c.* from 5% to 10%, and estimates for high 10-h FMC, *c.* 15%–25%, showed a large variance (Figure 7). The errors in the estimation by  $M_{FSMM}$  could also be confirmed in time series plots, which showed discrepancies, including those at a lower range of 10-h FMC (less than *c.* 10%).

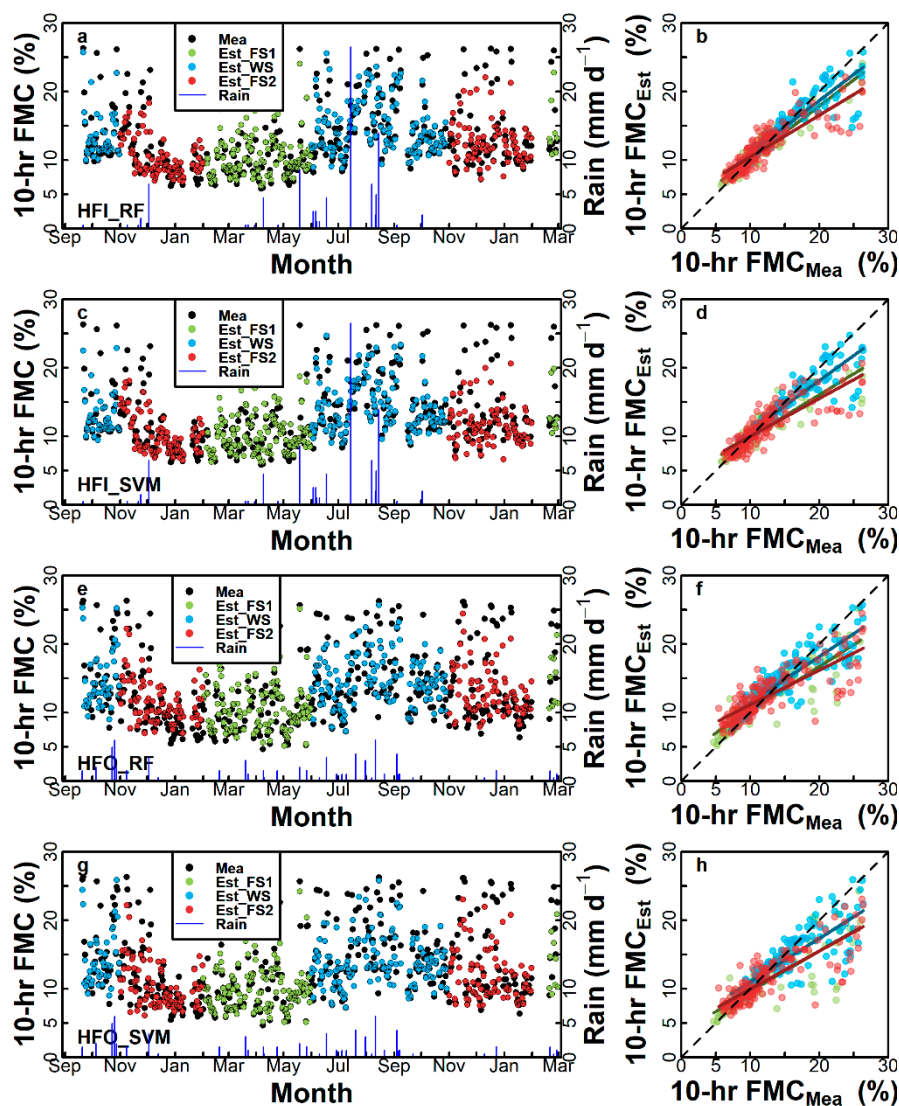


**Figure 6.** Time series and scatter plots comparing measurements (Mea) and estimates (Est) of 10-h fuel moisture content (10-h FMC) at HFI (a–d) and HFO (e–h) for each season: machine-learning models ( $M_{ML}$ ). FS1 refers to February through May; WS, to June through October; and FS2, to November through January. To greatly reduce the number of data points appearing on the graph, daily mean 10-h FMC values of the test dataset were used.

When evaluated against 10-h FMC below 10%, all models showed more variable performances and decreased RMSE and  $R^2$  (Figure 4e–h). RMSE ranged from 0.65% to 2.51% and from 0.86% to 4.27% in HFI and HFO, respectively. For both sites, the order of RMSE among the models, compared with that for the whole 10-h FMC range, only changed between RF and SVM. Nevertheless, the two models still showed distinctively better performance than the others.

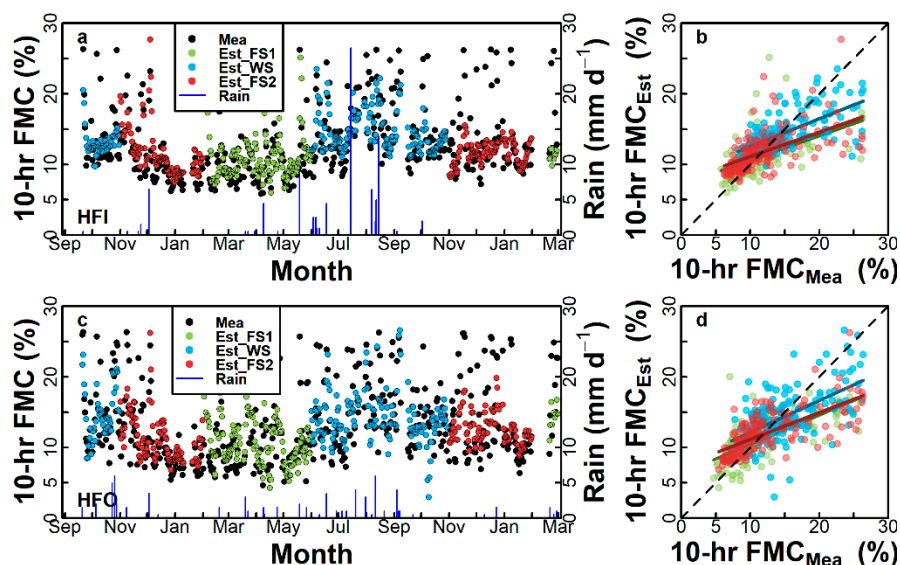


**Figure 7.** Time series and scatter plots comparing measurements (Mea) and estimates (Est) of 10-h fuel moisture content (10-h FMC) at HFI (a,b) and HFO (c,d) for each season: a process-based model ( $M_{FSMM}$ ). FS1 refers to February through May; WS, to June through October; and FS2, to November through January. To greatly reduce the number of data points appearing on the graph, daily mean 10-h FMC values of the test dataset were used.

### 3.4. Efficacy of the Seasonal Models

The development of separate seasonal models did not yield significant improvements in  $R^2$  and RMSE for any of the models (Figure 4). Generally,  $R^2$  values reduced and RMSE values increased with high variability in cases. In HFI, the average  $\pm$  standard deviation difference was  $-0.04 \pm 0.06$  in  $R^2$  and  $0.02 \pm 0.19\%$  in RMSE; in HFO, the corresponding differences were  $-0.02 \pm 0.03$  in  $R^2$  and  $0.04 \pm 0.25\%$  in RMSE. The same tendency appeared for 10-h FMC values less than 10% with larger differences and variabilities. Performance further decreased in terms of  $R^2$  ( $-0.04 \pm 0.18$  for HFI and  $-0.07 \pm 0.18$  for HFO) but increased in terms of RMSE ( $0.04 \pm 0.26\%$  for HFI and  $0.10 \pm 0.45\%$  for HFO).

## 4. Discussion

In contrast to weather condition proxies, 10-h dead FMC provides a direct measure of the dryness condition of fuels on the forest floor. This information can be used to improve existing models in the field of forest fires, such as those used for fire danger rating and fire behavior prediction. In this paper, five 10-h FMC models of three types were built, evaluated on the basis of measurements, and compared to each other. In this section, the performances and applicability of the models are discussed.

### 4.1. Model Performances

To start with, a possible limitation of the FS-3 fuel stick should be discussed. The inside of the FS-3 fuel stick sensor is hollowed out to allow for measurements of temperature and humidity inside it. However, in reality, the interior of 10-h fuels is not hollow. The sizeable volume of air space inside the fuel stick possibly made its measurements lower than the actual values. This limitation would not be related to the performances of  $M_{REG}$  and  $M_{ML}$  as these two models estimate 10-h FMC based on the observations by FS-3. On the other hand, the underestimation for high values by  $M_{FSMM}$  (Figure 7) could probably be attributed to this limitation as the model estimates are based solely on physical processes and not on FMC observations as with the other models. These limitations result in  $M_{FSMM}$  having a worse overall performance than the other models, as shown not only by the statistics (Figure 4) but also by the wider distribution of the estimates around 1:1 lines (compare Figures 5–7).

REG<sub>COR</sub> showed improved performance by including the CC as a predictor (Figure 4). The CC curve, which was adopted to calculate the CC, is a novel feature of this study. The degree of improvement in performances depended on the frequency of rainfall in the study site, since the CC aims to address errors that appeared after the end of rainfall, when the lagged response of the FMC to rapid changes in relative humidity occurred [7,10–12]. Lagged responses of litter moisture contents to meteorological factors (e.g., atmospheric temperature and relative humidity) have been reported by a number of studies e.g., [13,15]. This study adds evidence that 10-h FMC also shows a lagged response, similar to previous studies e.g., [10]. EMC is defined as the resultant FMC under constant relative humidity and temperature conditions after a sufficient amount of time has passed such that the fuel no longer gains or loses moisture [55]. EMC can be calculated from relative humidity and temperature (Equations (A1)–(A5)). Thus, fuels appear to require more time to reach the equilibrium moisture condition before and after rainfall, when the two conditions, especially the relative humidity, change rapidly. The degree of change in EMC occurring with changes in relative humidity is larger at high relative humidity than at the low values (e.g., Figure 1 in [11]). This may explain why the lagged response of FMC is apparent after the end of the rain event.

Two machine-learning algorithms based on SVM and RF were applied to FMC estimation for the first time in the present study. These two algorithms showed the best performances among the models evaluated in this study (Figure 4). This result confirms that machine-learning algorithms are applicable to FMC modeling. However, for these data-driven models based on machine-learning algorithms, it is difficult to obtain insights from their black-box processes. For example, the maximum and average wind direction were selected by the REF algorithm for all sites and learning methods (Table 3), but the underlying principle for the selection of these factors is uncertain. Therefore, hybrid modeling, which uses the data-driven (e.g., machine-learning) and process-driven (e.g., FSMM) approaches complementarily, as proposed by Reichstein et al. [56], is recommended.

The performance of  $M_{FSMM}$  was worse than that reported by van der Kamp et al. [9], who stated that FSMM showed an  $R^2$  of 0.90 and RMSE of 3.18% for 10-h fuel. This RMSE as well as  $R^2$  were much better than those obtained in the present study because van der Kamp et al. [9] used a 10-h FMC sensor with a higher upper limit (c. 60%) than that of the sensor used by this study (about 30%). Aside from the sensor differences, there might be two additional sources of errors for the poor performance of  $M_{FSMM}$  here. The first potential source was the input data. Downward shortwave radiation data are essential for running  $M_{FSMM}$ . Here, the radiation data were retrieved from the Seoul Meteorological Observatory, the nearest weather observatory since downward shortwave radiation was not observed at the study sites. This would lead to differences in the amount of radiation between the observatory and two study sites. Also, the two study sites would have different amounts in radiation because of shading effect of the pine canopy over HFI. These possible problems could have caused a significant amount of error. To investigate the extent of errors that could be caused by the uncertainty in radiation input, we analyzed the sensitivity of  $M_{FSMM}$  to radiation input by varying the radiation input over 10% intervals from 50% to 150% of the original value; the sensitivity was represented by the relative (i.e., the ratio of the difference from estimates with  $x\%$  radiation to estimates with 100% radiation) mean simulated 10-h FMC and the relative RMSE (Figure 8). The results showed that the relative mean 10-h FMC estimates varied from  $-9.48\%$  to  $11.47\%$  and from  $-7.90\%$  to  $9.37\%$  in HFI and HFO, respectively. Thus, the relative RMSE change ranged from  $-1.06\%$  to  $9.30\%$  and from  $-0.75\%$  to  $5.15\%$  in HFI and HFO, respectively. If radiation data were available for both sites, a significant amount of error would probably be removed.

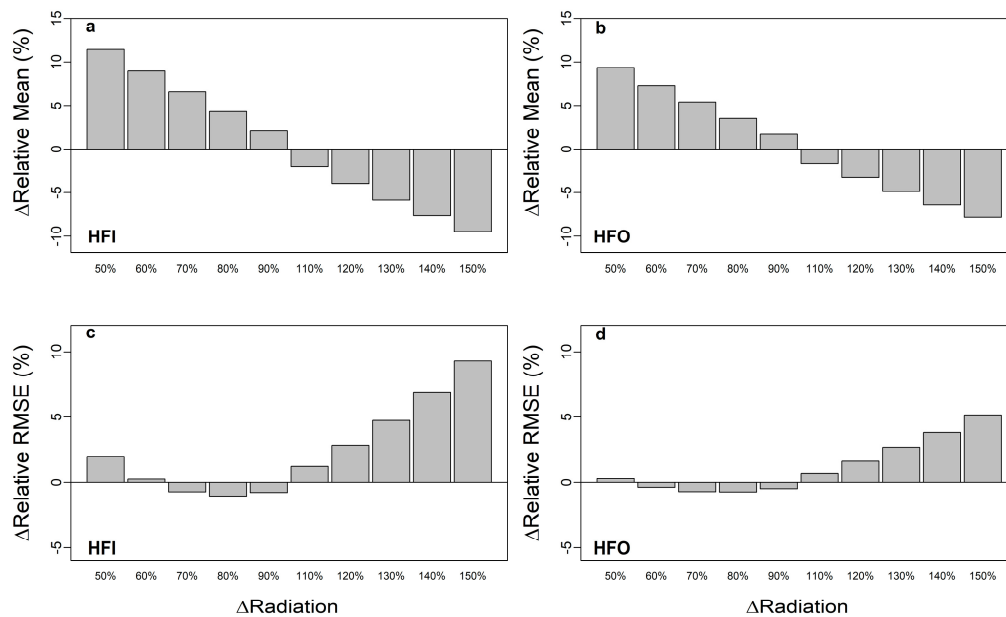


**Figure 8.** Results showing the sensitivity of 10-h fuel moisture content (10-h FMC) estimates obtained by the fuel stick moisture model (FSMM) to changes in shortwave downward radiation input for HFI (a,c) and HFO (b,d). “Relative” stands for the ratio of the difference in the statistics (a,b: mean and c,d: RMSE of 10-h FMC estimates) between estimates with 100% radiation and those with varied radiation to the statistics with 100% radiation. A positive y-value in each subplot indicates the increase in the relative statistics (i.e., relative mean and relative RMSE) compared to that with 100% radiation input.

The second potential source of errors was the difference in environmental conditions between the two studies (i.e., the more frequent rainfall events in HFI and HFO). The 10-h FMC usually shows abrupt changes when the atmospheric relative humidity changes rapidly, i.e., at the start and end of rainfall [10]. In addition to their own 5-month data set, van der Kamp et al. [9] also used a 21-month 10-h FMC dataset from the study by Carlson et al. [34], whose study sites showed less frequent rainfall events than HFI and HFO (over an 18-month period, HFI and HFO, respectively, had 144 and 179 rain events of more than 0.5-mm rainfall with duration longer than 1 h), which possibly reduced the performance of  $M_{FSMM}$  in the current study. For instance, Figure 5b in the study by van der Kamp et al. [9] shows underestimation for high 10-h FMC values. Although the monthly precipitation ranges were comparable among the three sites (0.5–173.7 mm for [34]; 0.0–188 mm for HFI; and 0.0–204.5 mm for HFO), the 10-h fuels in HFI and HFO would be more frequently saturated, given that the duration of rainfall had a greater influence on saturation than the rainfall intensity (Figure 3). Thus, the 10-h FMC would be more frequently underestimated in HFI and HFO.

The development of seasonal models yielded minimal improvement in RMSE and even decreased the  $R^2$  (Figure 4). This is due to the fact that 10-h FMC changes in direct response to the dynamic weather variables, a physical mechanism which is the same regardless of season. This finding may also imply that relationships between other variables (besides EMC) and 10-h FMC do not change across seasons. For instance, Resco de Dios et al. [33] built a 10-h FMC model using independent variables other than EMC (i.e., VPD) with the same equation for the whole year and reported a strong correlation ( $R^2 = 0.67$ ) with measurements.

#### 4.2. Applicability

All the models in this study are viable with a limited set of meteorological variables.  $M_{REG}$  requires only air temperature, relative humidity, and precipitation, which are commonly recorded variables. For  $M_{ML}$ , we examined 13 meteorological variables to optimize the model performance, and 9 to 13 variables were selected by RFE. However, the number of variables for  $M_{ML}$  can be further reduced if

required. For instance, the RFE with SVM in HFI selected all the 13 candidate variables, but  $R^2$  reduced by only 0.02 with the top five influential variables.

$M_{ML}$  showed the best performance among the models, but the machine would require periodic training using new measurements, necessitating large periods of time. Thus, the number of independent variables as described above may have to be reduced before applying the model to near real-time forecasting.  $REG_{COR}$  could be an alternative method with reasonable predictability ( $R^2 = 0.70$  and  $RMSE = 2.64\%$ ). However, the potential uncertainty is that the CC curve could differ among locations in the country given that Chow's test concluded that the two CC curves in HFI and HFO were different. However, the CC curve is used for determining CCs, which mostly increase the estimates for high 10-h FMC. The amount of increase would not affect the performance qualitatively; therefore, the difference in CC curves among locations may not present a significant problem.  $M_{FSMM}$  showed the worst performance in this study. For the reasons described above, however,  $M_{FSMM}$  should be reevaluated when the radiation input is available from the site where 10-h FMC is measured.

Since the 10-h FMC models introduced here utilize weather information as the input, a network of meteorological observatories can be deployed to synergize with the 10-h FMC models. The network will extend the spatial coverage of the simulation; the models will save the costs and times spent in installing 10-h FMC sensors at all stations in the network. For instance, NIFoS operates a system of meteorological observatories named the Automatic Mountain Meteorology Observation System (AMOS) [57]. Currently, AMOS consists of 313 observatories and spatially covers South Korea. This system can potentially be used as a source of fundamental weather data to estimate 10-h FMC because (1) dead fuel moisture is only controlled by the surrounding environmental conditions [2], (2) meteorological variables can be automatically observed by AMOS, and (3) AMOS is located at mountains with altitudes over 200 m [58], making it an appropriate data source since an observatory located on agricultural or urban land is not suitable for producing meteorological data for forest fire research or for operational systems such as fire danger rating [59].

## 5. Conclusions

We have compared the capability of various types of 10-h FMC model, including regression-, machine learning-, and process-based models. Our  $R^2$  results show that the machine learning-based models performed the best, followed by the regression models, with the process-based model doing the worst. The regression model was improved by incorporating a correction coefficient, which alleviates the significant errors in estimating high 10-h FMC. The machine learning-based model showed the best performance, but its interpretability was questionable, which calls for concurrent application of machine-learning and process-based models, i.e., the hybrid modeling approach. In general, whole-year models were only slightly better than seasonal models, as the physics of moisture response remains the same regardless of season. This study provides a new regression method for considering the lagged decrease in 10-h FMC after the end of rainfall, and the results of the model inter-comparisons will be useful for future fire modeling studies.

**Author Contributions:** Conceptualization, H.L. and M.W.; Data curation, H.L.; Formal analysis, H.L. and M.W.; Investigation, H.L.; Methodology, H.L. and M.W.; Project administration, M.W.; Supervision, M.W.; Validation, H.L.; Visualization, H.L.; Writing—original draft, H.L.; Writing—review and editing, H.L., M.W., S.Y. and K.J. All authors have read and agreed to the published version of the manuscript.

**Funding:** This research received no external funding.

**Acknowledgments:** The authors would like to thank Byungil Song and all the coworkers for maintaining the AMOS and collecting weather data.

**Conflicts of Interest:** The authors declare no conflict of interest.

## Appendix A

### A.1. Equilibrium Moisture Content (EMC)

EMC was calculated by the two-hydrate model [60,61]:

$$EMC (\%) = \frac{1800}{W} \left[ \frac{K_1 RH_a}{1 - K_1 RH_a} + \frac{K_1 K_2 RH_a + 2K_2 K_3 K_1^2 RH_a^2}{1 + K_1 K_2 RH_a + K_2 K_3 K_1^2 RH_a^2} \right] \quad (A1)$$

$$W = 349 + 1.29T_a + 0.0135T_a^2 \quad (A2)$$

$$K_1 = 0.805 + 0.000736T_a - 0.00000273T_a^2 \quad (A3)$$

$$K_2 = 6.27 - 0.00938T_a - 0.000303T_a^2 \quad (A4)$$

$$K_3 = 1.91 + 0.0407T_a - 0.000293T_a^2 \quad (A5)$$

### A.2. Effective Humidity (EH)

$$EH (\%) = \frac{RH_d + rRH_{d-1} + r^2RH_{d-2} + r^3RH_{d-3} + r^4RH_{d-4}}{1 + r + r^2 + r^3 + r^4} \quad (A6)$$

where  $RH_d$  indicates RH at day  $d$  and  $r$  is a constant (0.7).

### A.3. Vapor Pressure Deficit (VPD)

$$VPD (\text{kPa}) = ES(T_a) \times (100 - RH_a) \times 0.01 \quad (A7)$$

where  $ES(T_a)$  is saturated vapor pressure (kPa) at  $T_a$ , which is derived from the following equation [62]:

$$ES(T_a) = 0.611 \times \exp(17.27 \times T_a \div (T_a + 273.3)) \quad (A8)$$

### A.4. 10-H Fuel Moisture Content (10-H FMC)

The producer (FTS, Victoria, British Columbia, Canada) of the fuel stick sensor explains how to compute the 10-h FMC from temperature ( $T_s$ ) and relative humidity ( $RH_s$ ) inside the standard fuel stick:

$$RH_s < 10 : 10\text{-h FMC} = 0.03229 + 0.281073 \times RH_s - (0.0010404 \times RH_s \times T_s + 32)$$

$$10 \leq RH_s < 50 : 10\text{-h FMC} = 2.22749 + 0.160107 \times RH_s - 0.0266112(T_s + 32)$$

$$\begin{aligned} 50 \leq RH_s : 10\text{-h FM} \\ = 21.0606 + 0.005565 \times RH_s^2 - 0.483199 \times RH_s \\ - 0.00063 \times RH_s(T_s + 32) \end{aligned} \quad (A9)$$

## References

1. Thomas, P.A.; McAlpine, R.S. *Fire in the Forest*; Cambridge University Press: Cambridge, UK, 2010; ISBN 0-521-82229-7.
2. Bradshaw, L.S.; Deeming, J.E.; Burgan, R.E.; Cohen, J.D. *The 1978 National Fire-Danger Rating System: Technical Documentation*; Technical Report INT-169; USDA Forest Service General: Ogden, UT, USA, 1983.
3. Nieto, H.; Aguado, I.; Chuvieco, E.; Sandholt, I. Dead fuel moisture estimation with MSG-SEVIRI data. Retrieval of meteorological data for the calculation of the equilibrium moisture content. *Agric. For. Meteorol.* **2010**, *150*, 861–870. [[CrossRef](#)]
4. Jin, S.; Chen, P. Modelling drying processes of fuelbeds of Scots pine needles with initial moisture content above the fibre saturation point by two-phase models. *Int. J. Wildland Fire* **2012**, *21*, 418–427. [[CrossRef](#)]

5. Bakšić, N.; Bakšić, D.; Jazbec, A. Hourly fine fuel moisture model for *Pinus halepensis* (Mill.) litter. *Agric. For. Meteorol.* **2017**, *243*, 93–99.
6. Bilgili, E.; Coskuner, K.A.; Usta, Y.; Goltas, M. Modeling surface fuels moisture content in *Pinus brutia* stands. *J. For. Res.* **2019**, *30*, 577–587. [[CrossRef](#)]
7. Hiers, J.K.; Stauhammer, C.L.; O'Brien, J.J.; Gholz, H.L.; Martin, T.A.; Hom, J.; Starr, G. Fine dead fuel moisture shows complex lagged responses to environmental conditions in a saw palmetto (*Serenoa repens*) flatwoods. *Agric. For. Meteorol.* **2019**, *266*, 20–28. [[CrossRef](#)]
8. Nolan, R.H.; Resco de Dios, V.; Boer, M.M.; Caccamo, G.; Goulden, M.L.; Bradstock, R.A. Predicting dead fine fuel moisture at regional scales using vapour pressure deficit from MODIS and gridded weather data. *Remote Sens. Environ.* **2016**, *174*, 100–108. [[CrossRef](#)]
9. Van der Kamp, D.W.; Moore, R.D.; McKendry, I.G. A model for simulating the moisture content of standardized fuel sticks of various sizes. *Agric. For. Meteorol.* **2017**, *236*, 123–134. [[CrossRef](#)]
10. Lee, H.; Won, M.-S.; Yoon, S.-H.; Jang, K.-C. Modeling and mapping fuel moisture content using equilibrium moisture content computed from weather data of the automatic mountain meteorology observation system (AMOS). *J. Korean Assoc. Geogr. Inf. Stud.* **2019**, *22*, 21–36.
11. Matthews, S. Dead fuel moisture research: 1991–2012. *Int. J. Wildland Fire* **2014**, *23*, 78–92. [[CrossRef](#)]
12. Viney, N.R. A review of fine fuel moisture modelling. *Int. J. Wildland Fire* **1991**, *1*, 215–234. [[CrossRef](#)]
13. Catchpole, E.A.; Catchpole, W.R.; Viney, N.R.; McCaw, W.L.; Marsden-Smedley, J.B. Estimating fuel response time and predicting fuel moisture content from field data. *Int. J. Wildland Fire* **2001**, *10*, 215–222. [[CrossRef](#)]
14. Miller, E.A. Moisture sorption models for fuel beds of standing dead grass in Alaska. *Fire* **2019**, *2*, 2. [[CrossRef](#)]
15. Zhang, Y.; Sun, P. Study on the Diurnal Dynamic Changes and Prediction Models of the Moisture Contents of Two Litters. *Forests* **2020**, *11*, 95. [[CrossRef](#)]
16. Nelson, R.M., Jr. Prediction of diurnal change in 10-h fuel stick moisture content. *Can. J. For. Res.* **2000**, *30*, 1071–1087. [[CrossRef](#)]
17. Wittich, K.-P. A single-layer litter-moisture model for estimating forest-fire danger. *Meteorol. Z.* **2005**, *14*, 157–164. [[CrossRef](#)] [[PubMed](#)]
18. Matthews, S. A process-based model of fine fuel moisture. *Int. J. Wildland Fire* **2006**, *15*, 155–168. [[CrossRef](#)]
19. Fiorucci, P.; Gaetani, F.; Minciardi, R. Development and application of a system for dynamic wildfire risk assessment in Italy. *Environ. Model. Softw.* **2008**, *23*, 690–702. [[CrossRef](#)]
20. Matthews, S.; Gould, J.; McCaw, L. Simple models for predicting dead fuel moisture in eucalyptus forests. *Int. J. Wildland Fire* **2010**, *19*, 459–467. [[CrossRef](#)]
21. Lau, C.K.; Lai, K.K.; Lee, Y.P.; Du, J. Fire risk assessment with scoring system, using the support vector machine approach. *Fire Saf. J.* **2015**, *78*, 188–195. [[CrossRef](#)]
22. Nguyen, N.T.; Ngo, D.B.-T.; Xuan-Canh, P.; Hong-Thi, N.; Thi, B.H.; Nhat-Duc, H.; Dieu, T.B. Spatial pattern assessment of tropical forest fire danger at Thuan Chau area (Vietnam) using GIS-based advanced machine learning algorithms: A comparative study. *Ecol. Inform.* **2018**, *46*, 74–85.
23. Sayad, Y.O.; Mousannif, H.; Al Moatassime, H. Predictive modeling of wildfires: A new dataset and machine learning approach. *Fire Saf. J.* **2019**, *104*, 130–146. [[CrossRef](#)]
24. Jang, E.; Kang, Y.; Im, J.; Lee, D.-W.; Yoon, J.; Kim, S.-K. Detection and monitoring of forest fires using Himawari-8 geostationary satellite data in South Korea. *Remote Sens.* **2019**, *11*, 271. [[CrossRef](#)]
25. Massada, A.B.; Syphard, A.D.; Stewart, S.I.; Radeloff, V.C. Wildfire ignition-distribution modelling: A comparative study in the Huron–Manistee National Forest, Michigan, USA. *Int. J. Wildland Fire* **2013**, *22*, 174–183. [[CrossRef](#)]
26. Perry, G.L.; Wilmshurst, J.M.; McGlone, M.S.; Napier, A. Reconstructing spatial vulnerability to forest loss by fire in pre-historic New Zealand. *Glob. Ecol. Biogeogr.* **2012**, *21*, 1029–1041. [[CrossRef](#)]
27. Cabral, A.I.; Silva, S.; Silva, P.C.; Vanneschi, L.; Vasconcelos, M.J. Burned area estimations derived from Landsat ETM+ and OLI data: Comparing genetic programming with maximum likelihood and classification and regression trees. *ISPRS J. Photogramm. Remote Sens.* **2018**, *142*, 94–105. [[CrossRef](#)]
28. Collins, L.; Griffioen, P.; Newell, G.; Mellor, A. The utility of Random Forests for wildfire severity mapping. *Remote Sens. Environ.* **2018**, *216*, 374–384. [[CrossRef](#)]
29. Mithal, V.; Nayak, G.; Khandelwal, A.; Kumar, V.; Nemani, R.; Oza, N.C. Mapping burned areas in tropical forests using a novel machine learning framework. *Remote Sens.* **2018**, *10*, 69. [[CrossRef](#)]

30. Ramo, R.; García, M.; Rodríguez, D.; Chuvieco, E. A data mining approach for global burned area mapping. *Int. J. Appl. Earth Obs. Geoinf.* **2018**, *73*, 39–51. [[CrossRef](#)]
31. Won, M.-S.; Jang, K.-C.; Yoon, S.-H. Development of Fire Weather Index Model in Inaccessible Areas using MOD14 Fire Product and 5km-resolution Meteorological Data. *J. Korean Assoc. Geogr. Inf. Stud.* **2018**, *21*, 189–204.
32. Vinodkumar; Dharssi, I. Evaluation and calibration of a high-resolution soil moisture product for wildfire prediction and management. *Agric. For. Meteorol.* **2019**, *264*, 27–39. [[CrossRef](#)]
33. De Dios, V.R.; Fellows, A.W.; Nolan, R.H.; Boer, M.M.; Bradstock, R.A.; Domingo, F.; Goulden, M.L. A semi-mechanistic model for predicting the moisture content of fine litter. *Agric. For. Meteorol.* **2015**, *203*, 64–73. [[CrossRef](#)]
34. Carlson, J.D.; Bradshaw, L.S.; Nelson, R.M.; Bensch, R.R.; Jabrzemski, R. Application of the Nelson model to four timelag fuel classes using Oklahoma field observations: Model evaluation and comparison with National Fire Danger Rating System algorithms. *Int. J. Wildland Fire* **2007**, *16*, 204–216. [[CrossRef](#)]
35. Won, M.; Lee, S.; Lee, M.; Ohga, S. Development and application of a Forest fire danger rating system in South Korea. *J. Fac. Agric. Kyushu Univ.* **2010**, *55*, 221–229.
36. Chow, G.C. Tests of equality between sets of coefficients in two linear regressions. *Econom. J. Econom. Soc.* **1960**, *28*, 591–605. [[CrossRef](#)]
37. R Core Team. *R: A Language and Environment for Statistical Computing*; R Foundation for Statistical Computing: Vienna, Austria, 2019.
38. Zhao, J.H. A Genetic Analysis Package with R. *J. Stat. Softw.* **2007**, *23*, 1–18. [[CrossRef](#)]
39. Breiman, L. Random forests. *Mach. Learn.* **2001**, *45*, 5–32. [[CrossRef](#)]
40. James, G.; Witten, D.; Hastie, T.; Tibshirani, R. *An Introduction to Statistical Learning*; Springer: Berlin/Heidelberg, Germany, 2013; Volume 112.
41. Kuhn, M.; Johnson, K. *Applied Predictive Modeling*; Springer: Berlin/Heidelberg, Germany, 2013; Volume 26.
42. Kuhn, M.; Wing, J.; Weston, S.; Williams, A.; Keefer, C.; Engelhardt, A.; Cooper, T.; Mayer, Z.; Kenkel, B.; R Core Team; et al. Caret: Classification and Regression Training. CRAN–Package Caret. 2019. Available online: <https://CRAN.R-project.org/package=caret> (accessed on 9 September 2020).
43. Liaw, A.; Wiener, M. Classification and Regression by randomForest. *R News* **2002**, *2*, 18–22.
44. Vapnik, V.N. *The Nature of Statistical Learning*; Springer: New York, NY, USA, 1995.
45. Jakkula, V. Tutorial on Support Vector Machine (Svm). SVM Tutorial. Available online: <https://course.ccs.neu.edu/cs5100f11/resources/jakkula.pdf> (accessed on 9 September 2020).
46. Jeong, G.; Oeverdieck, H.; Park, S.J.; Huwe, B.; Lief, M. Spatial soil nutrients prediction using three supervised learning methods for assessment of land potentials in complex terrain. *Catena* **2017**, *154*, 73–84. [[CrossRef](#)]
47. Yao, Y.; Liang, S.; Li, X.; Chen, J.; Liu, S.; Jia, K.; Zhang, X.; Xiao, Z.; Fisher, J.B.; Mu, Q. Improving global terrestrial evapotranspiration estimation using support vector machine by integrating three process-based algorithms. *Agric. For. Meteorol.* **2017**, *242*, 55–74. [[CrossRef](#)]
48. Smola, A.J.; Schölkopf, B. A tutorial on support vector regression. *Stat. Comput.* **2004**, *14*, 199–222. [[CrossRef](#)]
49. Karatzoglou, A.; Smola, A.; Hornik, K.; Zeileis, A. Kernlab—An S4 Package for Kernel Methods in R. *J. Stat. Softw.* **2004**, *11*, 1–20. [[CrossRef](#)]
50. Guyon, I.; Elisseeff, A. An introduction to variable and feature selection. *J. Mach. Learn. Res.* **2003**, *3*, 1157–1182.
51. Guyon, I.; Weston, J.; Barnhill, S.; Vapnik, V. Gene selection for cancer classification using support vector machines. *Mach. Learn.* **2002**, *46*, 389–422. [[CrossRef](#)]
52. Van der Kamp, D.W. GitHub–Dvdkamp/Fsmm: Fuel Stick Moisture Model: Simulates Moisture Levels and Temperature for Standardized Fuel Sticks. Available online: <https://github.com/dvdkamp/fsmm> (accessed on 4 May 2020).
53. Bendtsen, C. *PSO: Particle Swarm Optimization*. CRAN–Package pso. 2012. Available online: <https://CRAN.R-project.org/package=pso> (accessed on 9 September 2020).
54. Won, M.; Yoon, S.; Jang, K. Developing Korean forest fire occurrence probability model reflecting climate change in the spring of 2000s. *Korean J. Agric. For. Meteorol.* **2016**, *18*, 199–207. [[CrossRef](#)]
55. Sharples, J.; McRae, R.; Weber, R.; Gill, A.M. A simple index for assessing fuel moisture content. *Environ. Model. Softw.* **2009**, *24*, 637–646. [[CrossRef](#)]

56. Reichstein, M.; Camps-Valls, G.; Stevens, B.; Jung, M.; Denzler, J.; Carvalhais, N. Deep learning and process understanding for data-driven Earth system science. *Nature* **2019**, *566*, 195–204. [[CrossRef](#)]
57. Mountain Weather Information System. Available online: <http://mtweather.nifos.go.kr/> (accessed on 4 May 2020).
58. Yoon, S.; Jang, K.; Won, M. The spatial distribution characteristics of Automatic Weather Stations in the mountainous area over South Korea. *Korean J. Agric. For. Meteorol.* **2018**, *20*, 117–126.
59. Aguado, I.; Chuvieco, E.; Boren, R.; Nieto, H. Estimation of dead fuel moisture content from meteorological data in Mediterranean areas. Applications in fire danger assessment. *Int. J. Wildland Fire* **2007**, *16*, 390–397. [[CrossRef](#)]
60. Hailwood, A.J.; Horrobin, S. Absorption of water by polymers: Analysis in terms of a simple model. *Trans. Faraday Soc.* **1946**, *42*, B084–B092. [[CrossRef](#)]
61. Ross, R.J. *Wood Handbook: Wood as an Engineering Material*; General Technical Report FPL-GTR-190; Forest Products Laboratory, USDA Forest Service: Madison, WI, USA, 2010; 509p.
62. Goyal, M.R. *Management of Drip/Trickle or Micro Irrigation*; CRC Press: Boca Raton, FL, USA, 2012.



© 2020 by the authors. Licensee MDPI, Basel, Switzerland. This article is an open access article distributed under the terms and conditions of the Creative Commons Attribution (CC BY) license (<http://creativecommons.org/licenses/by/4.0/>).